

Dynamical analysis, control, boundedness, and prediction for a fractional-order financial risk system

Kehao Yang(杨轲皓), Song Zheng(郑松), Tianhu Yu(余天虎), Aceng Sambas, Muhamad Deni Johansyah, Hassan Saberi-Nik, and Mohamad Afendee Mohamed

Citation: Chin. Phys. B, 2024, 33 (**11**): 110501. DOI: 10.1088/1674-1056/ad7afb
Journal homepage: http://cpb.iphy.ac.cn; http://iopscience.iop.org/cpb

What follows is a list of articles you may be interested in

Dynamical analysis, geometric control and digital hardware implementation of a complex-valued laser system with a locally active memristor

Yi-Qun Li(李逸群), Jian Liu(刘坚), Chun-Biao Li(李春彪), Zhi-Feng Hao(郝志峰), and Xiao-Tong Zhang(张晓彤)
Chin. Phys. B, 2023, 32 (**8**): 080503. DOI: 10.1088/1674-1056/acd68b

Dynamical analysis for the sustained harvesting of microorganisms using flocculants in a random environment

Rong Liu(刘蓉) and Wanbiao Ma(马万彪)
Chin. Phys. B, 2023, 32 (**5**): 050502. DOI: 10.1088/1674-1056/ac9367

Dynamical analysis, circuit realization, and application in pseudorandom number generators of a fractional-order laser chaotic system

Chenguang Ma(马晨光), Santo Banerjee, Li Xiong(熊丽), Tianming Liu(刘天明), Xintong Han(韩昕彤), and Jun Mou(牟俊)
Chin. Phys. B, 2021, 30 (**12**): 120504. DOI: 10.1088/1674-1056/abfbd4

Effect of magnetic flow and external forcing current on mixed bursting in the pre-Bötzinger complex

Dou-Dou Guo(郭豆豆), Zhuo-Sheng Lü(吕卓生)
Chin. Phys. B, 2019, 28 (**11**): 110501. DOI: 10.1088/1674-1056/ab43b9

Primary resonance of fractional-order Duffing-van der Pol oscillator by harmonic balance method

Sujuan Li(李素娟), Jiangchuan Niu(牛江川), Xianghong Li(李向红)
Chin. Phys. B, 2018, 27 (**12**): 120502. DOI: 10.1088/1674-1056/27/12/120502

Dynamical analysis, control, boundedness, and prediction for a fractional-order financial risk system

Kehao Yang(杨轲皓)[1], Song Zheng(郑松)[1,†], Tianhu Yu(余天虎)[2], Aceng Sambas[3,4], Muhamad Deni Johansyah[5], Hassan Saberi-Nik[6], and Mohamad Afendee Mohamed[3]

[1] *School of Data Science, Zhejiang University of Finance & Economics, Hangzhou* 310018, *China*
[2] *Department of Mathematics, Luoyang Normal University, Luoyang* 471934, *China*
[3] *Faculty of Informatics and Computing, Universiti Sultan Zainal Abidin, Besut Campus*, 22200, *Terengganu, Malaysia*
[4] *Department of Mechanical Engineering, Universitas Muhammadiyah Tasikmalaya, Tasikmalaya, Jawa Barat*, 46196, *Indonesia*
[5] *Department of Mathematics, Universitas Padjajdaran, Jatinangor, Kabupaten Sumedang* 45363, *Indonesia*
[6] *Department of Mathematics and Statistics, University of Neyshabur, Neyshabur* 9319774400, *Iran*

(Received 6 July 2024; revised manuscript received 6 September 2024; accepted manuscript online 14 September 2024)

This paper delves into the dynamical analysis, chaos control, Mittag–Leffler boundedness (MLB), and forecasting a fractional-order financial risk (FOFR) system through an absolute function term. To this end, the FOFR system is first proposed, and the adomian decomposition method (ADM) is employed to resolve this fractional-order system. The stability of equilibrium points and the corresponding control schemes are assessed, and several classical tools such as Lyapunov exponents (LE), bifurcation diagrams, complexity analysis (CA), and 0–1 test are further extended to analyze the dynamical behaviors of FOFR. Then the global Mittag–Leffler attractive set (MLAS) and Mittag–Leffler positive invariant set (MLPIS) for the proposed financial risk (FR) system are discussed. Finally, a proficient reservoir-computing (RC) method is applied to forecast the temporal evolution of the complex dynamics for the proposed system, and some simulations are carried out to show the effectiveness and feasibility of the present scheme.

Keywords: FOFR system, dynamical analysis, control, boundedness, forecasting

PACS: 05.45.–a, 05.45.Jn, 05.45.Pq **DOI:** 10.1088/1674-1056/ad7afb

1. Introduction

Since fractional-order calculus more close to reality, it has been adopted to model various biological, medical, chemical, and industrial phenomena, and so on.[1–5] In fact, fractional-order modeling provides a more dependable method for predicting, describing, and managing the behaviors of dynamic systems. Many works showed the fractional models, such as the recently developed hyperchaos complex system of fractional-order,[6] neural networks featuring hub structure, and multiple rings of fractional-order,[7] bank data model of -order integrating two unequal time delays,[8] fractional order monkeypox virus model,[9] and fractional buffering model,[10] could offer more accurate representations compared with their integer-order counterparts. Up to date, chaos in fractional-order dynamic systems, which exhibit some excellent and interesting dynamical behaviors, has been emerged as a fascinating subject for the researchers.[11–15]

Estimating the boundaries of solutions for chaotic systems is one of recently interesting focal points to investigate the dynamic behavior in a system. It is commonly known that the ultimate bounds and major dynamical system is crucial to be determined, in particular with practical considerations in locating hidden attractors, chaos synchronization, and chaos control.[16,17] Leonov[18,19] first proposed the computation of the Lorenz system's global bound. Later, Swinnerton–Dyer[20] applied Lyapunov functions to study the solution bounds of the Lorenz equations. Liao *et al.*[21] further designed a family of generalized Lyapunov functions, where they derived a positive invariant set of the Lorenz system and a new global attractive set by the application of synchronization and chaos control. Jian *et al.*[22] discussed the MLB and provided estimates of the global MLAS and MLPIS for a fractional-order chaotic system. Peng *et al.*[23] extended their exploration into the MLB and synchronization of fractional-order plasma chaotic systems, employing fractional differential inequalities and generalized Lyapunov functions. Ren *et al.*[24] employed the Lagrange coefficient method to establish a precise four-dimensional (4D) Rabinovich hyperchaotic system's ultimate bound set.

Chaotic economics, a recent theory within the realm of physical economics, can identify organized patterns and systematic behavior obscured within seemingly random economic phenomena. Many studies have explored the application of economic and FR models[25–28] by chaotic systems theory. Zhang *et al.*[25] constructed a risk management process of financial system, studied some interesting dynamical behaviors, and obtained the conditions for stability of the proposed system, respectively. Tacha *et al.*[26] investigated dynamical analysis, control, and circuit simulation of a financial

†Corresponding author. E-mail: szh070318@zufe.edu.cn

© 2024 Chinese Physical Society and IOP Publishing Ltd

system with an absolute function term. Furthermore, Tacha *et al.*[27] also discussed dynamical analysis of a fractional-order finance system with negative parameters. Jahanshahi *et al.*[28] examined the dynamical behavior of a 4D FR hyperchaotic system with variable-order fractional derivatives, and designed the predictive control scheme for suppressing the chaotic behavior while stabilizing the close-loop system. These investigations suggest that economics and financial systems adhere to a highly complex nonlinear system characteristics and cannot be simply modulated by integer-order calculus.

Recently, the time series forecasting has been employed in several fields including agriculture, commerce, biology, medicine, and so on.[29–31] There has been a proliferation of time series prediction methods in the field of artificial neural networks, such as recurrent neural networks (RNN), feedforward neural networks (FNN), and so on. Time series prediction has made extensive use of long short-term memory neural networks (LSTM), a unique kind of recurrent neural networks.[32,33] The improvement of LSTM network is the use of extra gates and better control over the processing information in the hidden units. Therefore, LSTM networks outperform traditional recurrent neural networks in their ability to learn long-term associations in time series and to predict sequence data. However, certain intricate nonlinear behaviors are challenging to handle by using LSTM networks and it has high computational costs. Due to the shortcomings of traditional recurrent neural networks, RC algorithm known as echo state network[34–36] has been developed. It is extensively applied in time series prediction because of its simpler structures, less computational costs, and higher accuracy. For example, Song *et al.*[37] implemented the RC algorithm for real-time power load forecasting, demonstrating superior predictive performance compared to FFNN. Na *et al.*[38] proposed a hierarchical echo state network with sparse learning and demonstrated the effectiveness based on experiments.

The motivation of this work can be summarized as follows: The financial risk system is characterized by variability and complexity. Traditional integer-order calculus has serious limitations in predicting and controlling the risks of the financial system and cannot accurately predict the time of occurrence and the degree of risk. Therefore, the application of fractional-order calculus is essential in the study of financial risk system. We delve deeper into the dynamical behavior and discuss LE, bifurcation diagrams, the C_0 algorithm,[39] SE algorithm,[40] and 0–1 test.[41] Then the global MLAS and MLPIS are studied. We also prove the attractiveness of the ultimate bound set of the proposed FOFR system. By modifying system parameters and other conditions, a multitude of attractive sets can be obtained. On the other hand, the prediction of financial risks is very favorable for the prevention and control of financial crises by an accurate and simpler algorithm like RC scheme. To our knowledge, the fractional dynamical behavior, MLB, and forecasting of the FOFR system with one absolute function term have not been studied thus far. Therefore, further in-depth study of the FOFR system with one absolute function term is warranted. The contributions of this paper are of four-fold.

(i) Proposing a fractional-order financial risk (FOFR) system featuring an absolute function term.

(ii) Investigating the dynamical analysis and complexity analysis using Lyapunov exponents, bifurcation analysis, 0–1 test, C_0, and SE.

(iii) The attractiveness of the ultimate bound set of the FOFR system is obtained.

(iv) An efficient RC approach is employed to predict the temporal evolution of the complicated dynamics.

The remainder of this paper is structured as follows. Section 2 presents some basic definitions, lemmas, and modelling. In Section 3, according to ADM, we investigate the stability analysis of equilibrium points and the dynamical behaviors in the proposed system, respectively. In Section 4, the linear controller will be designed to stabilize system at equilibrium points. Section 5 focuses on estimation of the global MLAS and MLPIS for the proposed system. Section 6 introduces the mathematical model for the RC technique along with numerical results. Furthermore, comparisons with the LSTM technique are conducted. The study is then summarized, and concluding remarks are provided in the last section.

2. Preliminaries and modeling

2.1. Preliminaries

Numerous definitions available out there for fractional order calculus,[1,2] such as Caputo, Riemann–Liouville, and Grunwald–Letnikov. In this work, we apply the Caputo definition. The following definitions apply to the Caputo integral and derivative in Refs. [1,2].

Definition 1[1,2] Given $f(t)$, its Caputo fractional integral can be defined as

$$ {}_{t_0}J_t^q f(t) = \frac{1}{\Gamma(q)} \int_{t_0}^{t} (t-s)^{q-1} f(s)\,\mathrm{d}s, $$

where $\Gamma(\cdot)$ is a gamma function, and $t \geq t_0$, $q > 0$.

Definition 2[1,2] The Caputo fractional derivative of order q is given as follows:

$$ {}_{t_0}^{C}D_t^q f(t) = \frac{1}{\Gamma(m-q)} \int_{a}^{t} (t-s)^{m-q-1} f^{(m)}(s)\,\mathrm{d}s, $$

where $m-1 < q < m$, t_0 and t are integers that indicate the operator's bounds. ${}_{t_0}^{C}D_t^q$. Also, when $0 < q < 1$, the fractional-order derivative of $f(t)$ can be concluded as

$$ {}_{t_0}^{C}D_t^q f(t) = \frac{1}{\Gamma(1-q)} \int_{a}^{t} (t-s)^{-q} f'(s)\,\mathrm{d}s. $$

Definition 3[1,2] The following equations defines two parameters Mittag–Leffler function:

$$E_{p,q}(m)=\sum_{k=0}^{\infty}\frac{m^k}{\Gamma(kp+q)},$$

for some complex number m. Simple operation gives

$$E_p(m)=E_{p,1}(m),\quad E_{0,1}(m)=\frac{1}{1-m},\quad E_{1,1}(m)=\mathrm{e}^m.$$

Definition 4[22] Consider the Lyapunov function $V_\lambda(t)=V_\lambda(x(t))$with $\lambda>0$, if there exist constants $L_\lambda>0$, $r_\lambda>0$, and $x_0\in R^m$ such that

$$V_\lambda(t)-L_\lambda\le(V_\lambda(t_0)-L_\lambda)E_q(-r_\lambda(t-t_0)^q),$$

for $t\ge t_0$, $V_\lambda(t_0)>L_\lambda$, $V_\lambda(t)>L_\lambda$, then the set $\Psi_\lambda=\{x(t)\in R^m|V_\lambda(x(t))\le L_\lambda\}$ is said to be a global MLAS of the system. If for any $t>t_0$, $x(t,t_0,x_0)\in\Psi_\lambda$, $t>t_0$, or $x_0\in\Psi_\lambda$, then Ψ_λ is said to be an MLPIS, where $x(t)=(x_1,x_2,\ldots,x_m)^{\mathrm{T}}$,$x_0=x(t_0)$.

Lemma 1[3] Consider a nonlinear dynamical system of fractional-order ${}_{t_0}^{C}D_t^q x(t)=f(x(t))$, with $0<q<1$, $x(t)\in R^m$, and $f(x(t))$as a continuous differential nonlinear function. Moreover, let a respective Jacobian matrix $J=\partial f/\partial x$ with eigenvalues λ_i at the equilibrium point, if all eigenvalues satisfy $|\arg(\lambda_i)|>q\pi/2$, where $i=1,2,\ldots,m$, then the system is local asymptotic stability.

Lemma 2[22] Let $f(t)\in R$ be a smooth function, then ${}_{t_0}^{C}D_t^q(f^2(t))\le 2f(t){}_{t_0}^{C}D_t^q(f(t))$, $t\ge t_0$, $0<q<1$.

Lemma 3[22] Let $q\in(0,1)$ and a constant $K\in R$. If a continuous function $f(t)$ satisfies ${}_{t_0}^{C}D_t^q(f(t))\le Kf(t)$, then $f(t)\le f(0)E_q(Kt^q)$, for the case of $t\ge 0$.

2.2. Modeling

Muhamad Deni Johansyah *et al.*[42] proposed a new FR system can be defined as

$$\begin{cases}\dot{x}_1=a(x_2-x_1),\\ \dot{x}_2=bx_1-x_2-x_1x_3-c|x_2|,\\ \dot{x}_3=x_1x_2-dx_3,\end{cases}\tag{1}$$

where $\{x_1,x_2,\text{and}\,x_3\}=\{$occurrence value risk, analysis value risk, and control value risk$\}$ for the current market. Inspired by the integer-order FR system in Ref. [42]. This study applies the Caputo fractional derivative operator to the system (1). Consequently we can derive the FR system in the form of fractional-order differential equations as follows:

$$\begin{cases}{}_{t_0}^{C}D_t^q x_1=a(x_2-x_1),\\ {}_{t_0}^{C}D_t^q x_2=bx_1-x_2-x_1x_3-c|x_2|,\\ {}_{t_0}^{C}D_t^q x_3=x_1x_2-dx_3,\end{cases}\tag{2}$$

where $q\in(0,1)$ represents the order of derivative. In case of $q=1$, system (2) degenerates into an integer-order differential equation. An approximate solution by using the ADM[43] to the FOFR system (2) can be simplified into the following equation:

$$\begin{aligned}\tilde{x}_j=\;&b_j^0+b_j^1\frac{(t-t_0)^q}{\Gamma(q+1)}+b_j^2\frac{(t-t_0)^{2q}}{\Gamma(2q+1)}+\cdots\\&+b_j^6\frac{(t-t_0)^{6q}}{\Gamma(6q+1)},\end{aligned}\tag{3}$$

where $j=1,2,3$, while the detailed derivation of $b_j^1,b_j^2,\ldots,b_j^6$ is available in Appendix A.

Based on this approximate solution, when $h=0.01$, $q=0.98$, $a=10$, $b=28$, $c=0.4$, $d=8/3$ with the initial values (10,10,10), the phase diagram of the FOFR system (2) can be obtained as shown in Fig. 1, which exhibits chaotic characteristics.

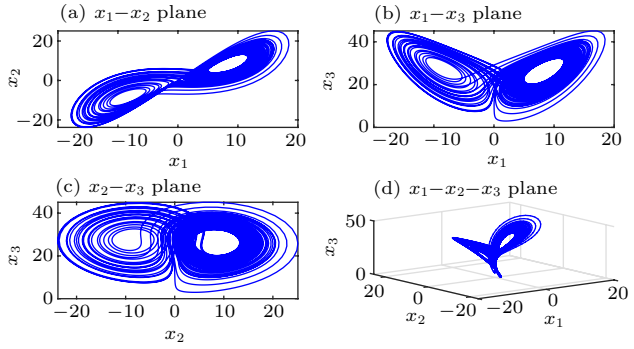


Fig. 1. Phase diagrams of FOFR system (2) when $q=0.98$, $a=10$, $b=28$, $c=0.4$, $d=8/3$.

2.3. Stability analysis of equilibrium points

To solve the equilibrium points for system (2), let

$$\begin{cases}a(x_2-x_1)=0,\\ bx_1-x_2-x_1x_3-c|x_2|=0,\\ x_1x_2-dx_3=0,\end{cases}\tag{4}$$

we obtain a better understanding of the system's dynamics by solving Eq. (4).

When $x_2>0$, if $bd-d-cd<0$, the system has a unique equilibrium point $E_1=(0,0,0)$;$bd-d-cd\ge 0$, the system has two equilibrium points $E_1=(0,0,0)$ and $E_2=(\sqrt{bd-d-cd},\sqrt{bd-d-cd},b-c-1)$.

When $x_2<0$, if $bd-d+cd<0$, the system has a unique equilibrium point $E_1=(0,0,0)$; $bd-d+cd\ge 0$, the system has two equilibrium points $E_1=(0,0,0)$, $E_2=(-\sqrt{bd-d+cd},-\sqrt{bd-d+cd},b+c-1)$.

To summarize, there are three equilibrium points when the conditions are satisfied:

$$\begin{aligned}&E_1=(0,0,0),\\&E_2=\left(\sqrt{bd-d-cd},\sqrt{bd-d-cd},b-c-1\right),\\&E_3=\left(-\sqrt{bd-d+cd},\ -\sqrt{bd-d+cd},b+c-1\right).\end{aligned}$$

By considering $a=10$, $b=28$, $c=0.4$, and $d=8/3$ such that $bd-d-cd\ge 0$, $bd-d+cd\ge 0$, system (2) exhibits the three equilibrium points to be

$$E_1=(0,0,0),\quad E_2=(8.4221,8.4221,26.6),$$

$$E_3 = (-8.5479, -8.5479, 27.4). \tag{5}$$

The Jacobian matrix of the system (2) at the equilibrium point of E^* is

$$J = \begin{bmatrix} -a & a & 0 \\ b - x_3^* & -1 - c \times \text{sign}(x_2^*) & -x_1^* \\ x_2^* & x_1^* & -d \end{bmatrix}. \tag{6}$$

By substituting $E_1 = (0,0,0)$ into the Jacobian matrix (6), the eigenvalues are $\lambda_1 = 11.828$, $\lambda_2 = 2.667$, $\lambda_3 = -22.828$. By Lemma 1, we have $|\arg(\lambda_1)| = 0$, $|\arg(\lambda_2)| = 0$, and $|\arg(\lambda_3)| = \pi$, therefore E_1 is said to be unstable.

By substituting $E_2 = (8.4221, 8.4221, 26.6)$ into the Jacobian matrix (6), the eigenvalues are $\lambda_1 = -14.044, \lambda_{2,3} = -0.0113132 \pm 10.0506\text{i}$. By Lemma 1, we obtain $|\arg(\lambda_1)| = \pi$ and $|\arg(\lambda_2)| = |\arg(\lambda_3)| = 1.5719$, hence E_2 is locally asymptotically stable.

By substituting $E_3 = (-8.5479, -8.5479, 27.4)$ into the Jacobian matrix (6), the eigenvalues are $\lambda_1 = -13.6725, \lambda_{2,3} = 0.202887 \pm 10.3364\text{i}$, so we have $|\arg(\lambda_1)| = \pi$, $|\arg(\lambda_2)| = 1.5506$, $|\arg(\lambda_3)| = 1.5506$, by Lemma 1, E_3 is local asymptotic stability when $q < 2|\arg(\lambda_{2,3})|/\pi = 0.9871$.

3. Dynamical analysis of the FOFR system

This section analyzes the dynamical properties of the proposed model in relation to its parameters. We examine the equilibrium point characteristics by utilizing various techniques based on bifurcation diagram and LE. The FOFR system (2) exhibits a range of dynamic behaviors that includes stable, periodic, and chaotic motions.

3.1. Bifurcation diagram and Lyapunov exponent

3.1.1. Let $\{a,b,c,q\} = \{10,28,0.4,0.98\}$ and d varies

Figures 2 and 3 respectively depict the bifurcation diagram and spectrum of LE when d takes the values between $[0,3.5]$. When $d \in (0.15,0.5)$, the system exhibits periodic behavior and has two negative LE and one zero LE. When $d \in (0,0.15) \cup (0.5,3.2)$, the system exhibits one positive LE which concludes the chaoticity of the system. When $d \in (3.2,3.5)$, there are three negative LEs which means the system is stable.

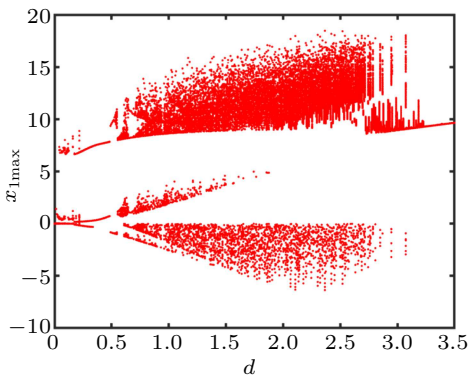


Fig. 2. Bifurcation illustration of system with d when $a = 10$, $b = 28$, $c = 0.4$, $q = 0.98$.

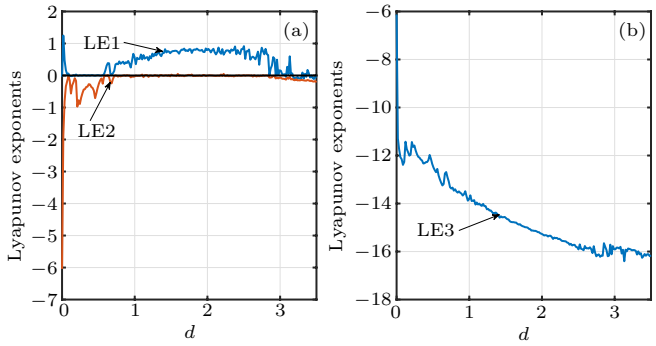


Fig. 3. Lyapunov exponent spectra with d when $a = 10$, $b = 28$, $c = 0.4$, $q = 0.98$.

3.1.2. Let $\{a,b,c,d\} = \{10,28,0.4,8/3\}$ and q varies

Following a similar approach, we conduct further analysis by varying parameter q. The bifurcation diagram is displayed in Fig. 4 when the parameter $q \in (0.75,1)$ is considered. It can be observed that the system exhibits a stable state when $q \in (0.75,0.93)$, while it demonstrates chaotic behavior when $q \in (0.93,1)$. Additionally, the LE spectrum shown in Fig. 5 confirms the chaotic nature of the system, aligning with the findings from the bifurcation diagram. Specifically, when $q \in (0.75,0.93)$, all three LEs are negative, indicating a stable state. However, when $q \in (0.93,1)$, the system displays chaos with one positive LE.

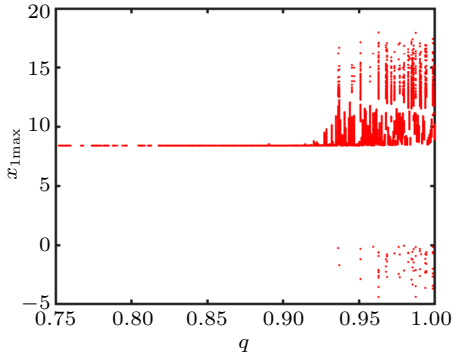


Fig. 4. Bifurcation illustration with q when $a = 10$, $b = 28$, $c = 0.4$, $d = 8/3$.

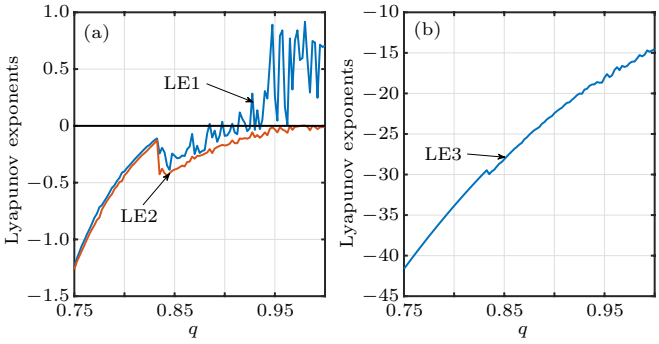


Fig. 5. Lyapunov exponent spectra with q when $a = 10$, $b = 28$, $c = 0.4$, $d = 8/3$.

3.2. Complexity analysis

3.2.1. Let $\{a,b,c,q\} = \{10,28,0.4,0.98\}$ and d varies

By varying d, the phase portraits and the p–s dynamics of the 0–1 test are plotted as in Fig. 6. Apparently, the system exhibits periodicity when $d = 0.15$. When $d = 2$ and $d = 3.3$, the system is chaotic and stable. It shows that the system goes through periodic behavior and becomes gradually stable as d improves. Additionally, results from numerical imaging corroborate with the C and SE algorithms, found in Fig. 7.

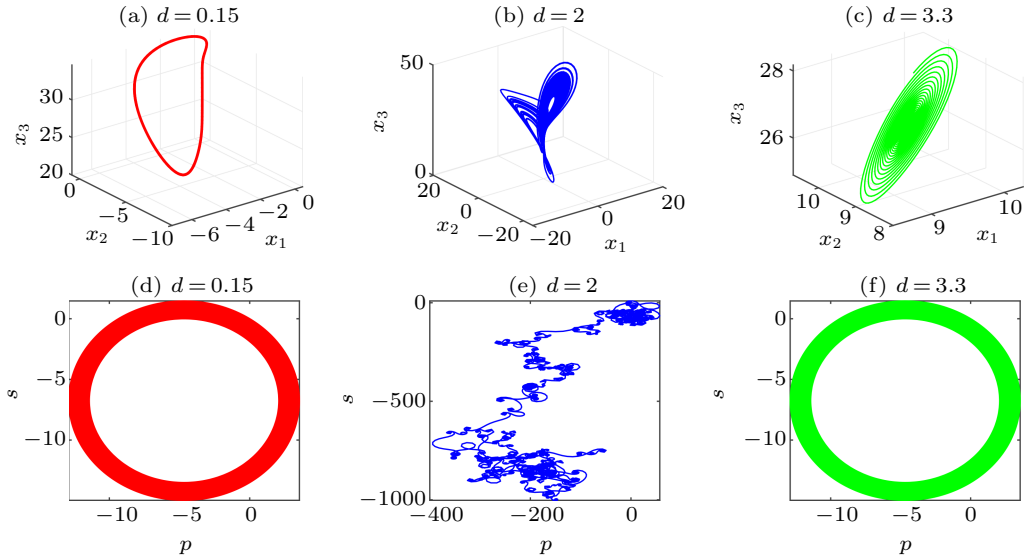


Fig. 6. Phase portraits and the p–s plots of the 0–1 test for the system when $a = 10$, $b = 28$, $c = 0.4$, [(a) and (d)] $d = 0.15$; [(b) and (e)] $d = 2$; [(c) and (f)] $d = 3.3$.

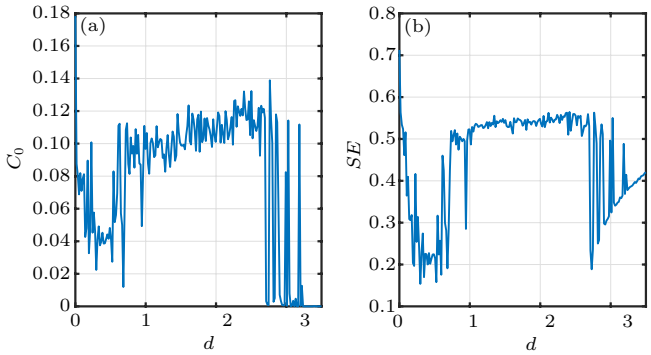


Fig. 7. (a) C_0 and (b) SE complexity of the system with d when $a = 10$, $b = 28$, $c = 0.4$, $q = 0.98$.

3.2.2. Let $\{a,b,c,d\} = \{10,28,0.4,8/3\}$ and q varies

Figure 8 provides phase portraits and p–s dynamics using the 0–1 test for specific values of q. It can be observed that the system exhibits chaos when $q = 0.94$ and $q = 0.98$, while it shows stable behavior when $q = 0.84$. Furthermore, figure 9 presents the C_0 and SE complexity values belonging to system (2). Given smaller values of $q \in (0.75, 0.93)$, the complexity values are low, whereas oscillations are observable at higher values of $q \in (0.93, 1)$. This suggests that as the parameter q improves, the system gradually becomes more chaotic. It indicates that as the fractional order q gradually increases,

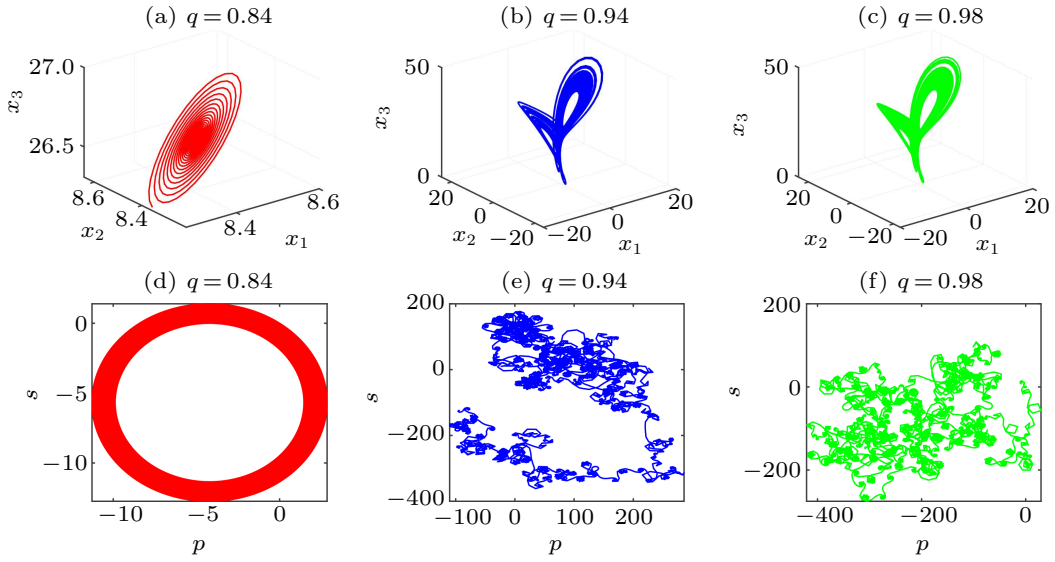


Fig. 8. Phase portraits and the p–s plots of the 0–1 test for the system when $a = 10$, $b = 28$, $c = 0.4$, [(a) and (b)] $q = 0.84$; [(b) and (e)] $q = 0.94$; [(c) and (f)] $q = 0.98$.

the financial system is out of control and more damaging to the economy. Figure 10 shows the corresponding time series diagram of the system. As shown in figure, the smaller the order q, the faster the system reaches the stable state and the occurrence value risk fluctuate in the smaller range. In practice, this means that financial risks that spread on a small scale can be effectively controlled in a relatively short period of time. Thus, it indicates that the fraction-order system more accurately reflects the real-world financial risk system compared to integer-order one.

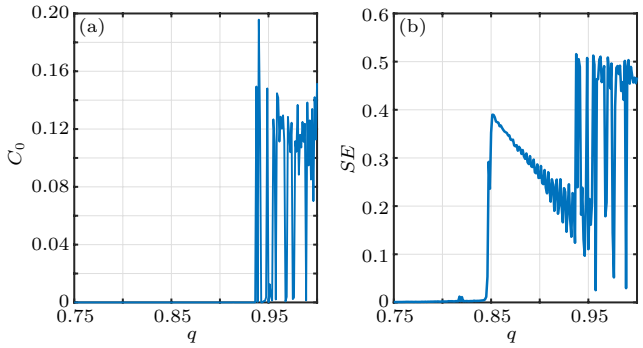


Fig. 9. (a) C_0 and (b) SE complexity of the system with q when $a = 10$, $b = 28$, $c = 0.4$, $d = 8/3$.

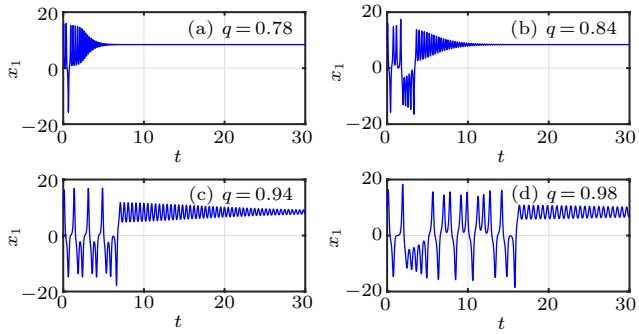


Fig. 10. Time series of state x_1 when $a = 10$, $b = 28$, $c = 0.4$, $d = 8/3$; (a) $q = 0.78$, (b) $q = 0.84$, (c) $q = 0.9$, (d) $q = 0.98$.

4. Chaos control

This section begins with the employment of linear feedback control method for the purpose of stabilizing system (2) towards its equilibrium points. In so doing, consider the following system:

$$\begin{cases} D^q_{t_0} x_1 = a(x_2 - x_1) - w_1(x_1 - x_1^*), \\ D^q_{t_0} x_2 = b x_1 - x_2 - x_1 x_3 - c\,|x_2| - w_2(x_2 - x_2^*), \\ D^q_{t_0} x_3 = x_1 x_2 - d x_3 - w_3(x_3 - x_3^*), \end{cases} \tag{7}$$

where w_1, w_2, w_3 are control parameters and E^* is the equilibrium point of the system (2).

The Jacobian matrix of the system (7) at the equilibrium point of E^* is

$$J(E^*) = \begin{bmatrix} -a - w_1 & a & 0 \\ b - x_3^* & -1 - c \times \mathrm{sign}(x_2^*) - w_2 & -x_1^* \\ x_2^* & x_1^* & -d - w_3 \end{bmatrix}. \tag{8}$$

For this Jacobian matrix $J(E^*)$, its characteristics equation is given by

$$f(\lambda) = \begin{vmatrix} \lambda + a + w_1 & -a & 0 \\ -b + x_3^* & \lambda + 1 + c\mathrm{sign}\,(x_2^*) + w_2 & x_1^* \\ -x_2^* & -x_1^* & \lambda + d + w_3 \end{vmatrix}. \tag{9}$$

When $a = 10$, $b = 28$, $c = 0.4$, $d = 8/3$, we first select $w_1 = 12$, $w_2 = 14$, $w_3 = 10$ to stabilize system (2) at equilibrium point $E_1(0,0,0)$. The characteristic polynomial is given as

$$f(\lambda) = \lambda^3 + \frac{149}{3}\lambda^2 + \frac{2408}{3}\lambda + \frac{12692}{3}, \tag{10}$$

then, the eigenvalues of the characteristic polynomial (10) are $\lambda_1 = -35.5953$, $\lambda_2 = -1.4047$, $\lambda_3 = -12.6667$. Since $|\arg(\lambda_1)| = |\arg(\lambda_2)| = |\arg(\lambda_3)| = \pi$, the equilibrium point $E_1(0,0,0)$ is locally asymptotically stable for all $0 < q < 1$. Furthermore, in order to get a simpler control scheme, we can consider the case where one control parameter is 0 or two control parameters are 0. Therefore, we can choose $w_1 = 18$, $w_2 = 20$, $w_3 = 0$ or $w_1 = 0$, $w_2 = 62$, $w_3 = 0$. The eigenvalues of the Jacobian matrix (8) are $\lambda_1 = -41.5953$, $\lambda_2 = -7.4047$, $\lambda_3 = -2.6667$ and $\lambda_1 = -5.1591$, $\lambda_2 = -67.8409$, $\lambda_3 = -2.667$, respectively. Since $|\arg(\lambda_1)| = |\arg(\lambda_2)| = |\arg(\lambda_3)| = \pi$, the equilibrium point $E_1(0,0,0)$ is local asymptotic stability for all $0 < q < 1$ in both cases.

The effectiveness of the designed control method is demonstrated in Figs. 11–13. These figures indicate that the designed controllers are capable of effectively controlling chaos in the FOFR system (2). Moreover, as the fractional order decreases, the system appears to move much more rapidly towards the equilibrium point $E_1(0,0,0)$.

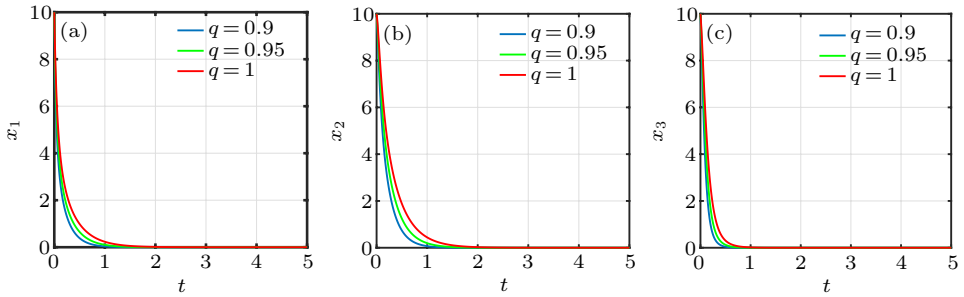


Fig. 11. Time series of the controlled system (7) with the fractional order $q = 0.9$, $q = 0.95$, $q = 1$ when $w_1 = 12$, $w_2 = 14$, $w_3 = 10$.

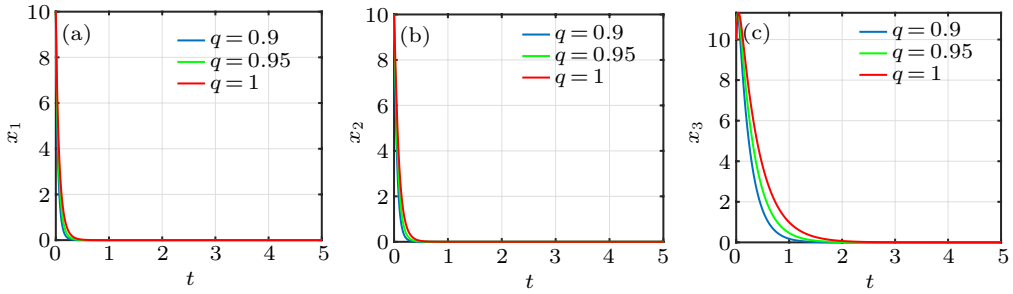


Fig. 12. Time series of the controlled system (7) with the fractional order $q=0.9$, $q=0.95$, $q=1$ when $w_1=18$, $w_2=20$, $w_3=0$.

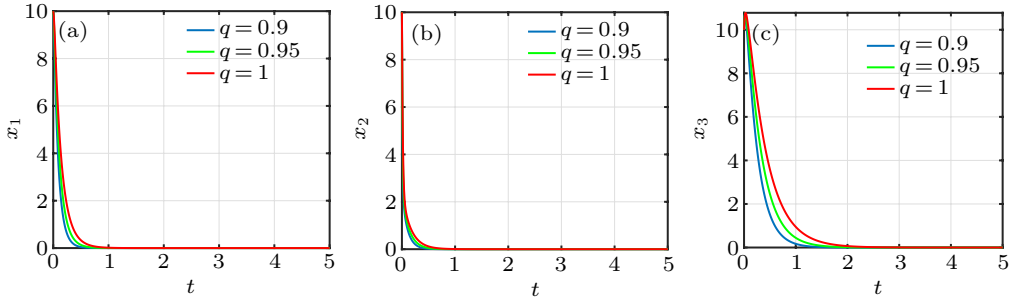


Fig. 13. Time series of the controlled system (7) with the fractional order $q=0.9$, $q=0.95$, $q=1$ when $w_1=0$, $w_2=62$, $w_3=0$.

5. Boundedness of the FOFR system

In this section, we will estimate the global MLAS and MLPIS for the proposed system (2).

Theorem 1 When $x_2>0$, let $a>0$, $c>-1$, $d>0$, $\lambda_1>0$, $\mu_1>\lambda_1 b$, the global MLAS and MLPIS of system (2) is as follows:

$$\Psi^1_{\lambda_1,\mu_1} = \left\{x(t)\in R^3 \left| \frac{\mu_1-\lambda_1 b}{a}x_1^2+\lambda_1 x_2^2 + \lambda_1\left(x_3-\frac{\mu_1}{\lambda_1}\right)^2 \le T^2_{1\max}\right.\right\}, \tag{11}$$

where

$$T^2_{1\max}=\frac{d\mu_1^2}{\lambda_1\eta_1}, \quad \eta_1=\min\{a,1+c,d\}>0. \tag{12}$$

When $x_2<0$, let $a>0$, $c<1$, $d>0$, $\lambda_2>0$, $\mu_2>\lambda_2 b$, the global MLAS and MLPIS of system (2) is as follows:

$$\Psi^2_{\lambda_2,\mu_2} = \left\{x(t)\in R^3 \left| \frac{\mu_2-\lambda_2 b}{a}x_1^2+\lambda_2 x_2^2 + \lambda_2\left(x_3-\frac{\mu_2}{\lambda_2}\right)^2 \le T^2_{2\max}\right.\right\}, \tag{13}$$

where

$$T^2_{2\max}=\frac{d\mu_2^2}{\lambda_2\eta_2}, \quad \eta_2=\min\{a,1-c,d\}>0. \tag{14}$$

Proof When $x_2>0$, specify the subsequent generalized Lyapunov function, which is both positively definite and radically unbounded

$$V_{\lambda_1,\mu_1}(x_1,x_2,x_3) = \frac{1}{2}\frac{\mu_1-\lambda_1 b}{a}x_1^2+\frac{1}{2}\lambda_1 x_2^2+\frac{1}{2}\lambda_1\left(x_3-\frac{\mu_1}{\lambda_1}\right)^2, \tag{15}$$

where $\lambda_1>0$, $\mu_1>0$. By applying the fractional derivative to V_{λ_1,μ_1} and using Lemma 2, we can obtain

$$\begin{aligned} D_t^q V_{\lambda_1,\mu_1}(x(t)) &\le (\mu_1-\lambda_1 b)x_1 D_t^q x_1+\lambda_1 x_2 D_t^q x_2 \\ &\quad +\lambda_1\left(x_3-\frac{\mu_1}{\lambda_1}\right)D_t^q x_3 \\ &= -\frac{1}{2}(\mu_1-\lambda_1 b)x_1^2-\frac{1}{2}\lambda_1(1+c)x_2^2 \\ &\quad -\frac{1}{2}d\lambda_1\left(x_3-\frac{\mu_1}{\lambda_1}\right)^2+F(x(t)), \end{aligned} \tag{16}$$

where

$$\begin{aligned} F(x(t)) &= -\frac{1}{2}(\mu_1-\lambda_1 b)x_1^2-\frac{1}{2}\lambda_1(1+c)x_2^2 \\ &\quad -\frac{1}{2}d\lambda_1 x_3^2+\frac{1}{2}\frac{d\mu_1^2}{\lambda_1}. \end{aligned} \tag{17}$$

Evidentially,

$$F(x(t))\le \sup F(x(t))=l_{\lambda_1,\mu_1}=\frac{1}{2}\frac{d\mu_1^2}{\lambda_1},$$

we have

$$D_t^q V_{\lambda_1,\mu_1}(x(t))\le -\eta_1 V_{\lambda_1,\mu_1}+l_{\lambda_1,\mu_1}, \tag{18}$$

$$D_t^q\left(V_{\lambda_1,\mu_1}(t)-\frac{l_{\lambda_1,\mu_1}}{\eta_1}\right)\le -\eta_1\left(V_{\lambda_1,\mu_1}-\frac{l_{\lambda_1,\mu_1}}{\eta_1}\right). \tag{19}$$

According to Lemma 3, we have

$$V_{\lambda_1,\mu_1}(t)-\frac{l_{\lambda_1,\mu_1}}{\eta_1}\le\left(V_{\lambda_1,\mu_1}(0)-\frac{l_{\lambda_1,\mu_1}}{\eta_1}\right)E_q(-\eta_1 t^q), \quad t\ge 0. \tag{20}$$

Based on Definition 4, we can conclude that $\Psi^1_{\lambda_1,\mu_1}$ with $a>0$, $c>-1$, $d>0$, $\lambda_1>0$, $\mu_1>\lambda_1 b$ is an MLAS and MLPIS for system (2) when $x_2>0$.

When $x_2 < 0$, choose the following Lyapunov function:

$$V_{\lambda_2,\mu_2}(x_1,x_2,x_3) = \frac{1}{2}\frac{\mu_2-\lambda_2 b}{a}x_1^2+\frac{1}{2}\lambda_2 x_2^2 + \frac{1}{2}\lambda_2\left(x_3-\frac{\mu_2}{\lambda_2}\right)^2, \tag{21}$$

where $\lambda_2 > 0, \mu_2 > 0$. By applying the fractional derivative to V_{λ_2,μ_2} and using Lemma 2, we can obtain

$$\begin{aligned} D_t^q V_{\lambda_2,\mu_2}(x(t)) &\le (\mu_2-\lambda_2 b)x_1 D_t^q x_1+\lambda_2 x_2 D_t^q x_2 \\ &\quad +\lambda_2\left(x_3-\frac{\mu_2}{\lambda_2}\right)D_t^q x_3 \\ &= -\frac{1}{2}(\mu_2-\lambda_2 b)x_1^2-\frac{1}{2}\lambda_2(1-c)x_2^2 \\ &\quad -\frac{1}{2}\lambda_2 d\left(x_3-\frac{\mu_2}{\lambda_2}\right)^2+F(x(t)), \end{aligned} \tag{22}$$

where

$$\begin{aligned} F(x(t)) &= -\frac{1}{2}(\mu_2-\lambda_2 b)x_1^2-\frac{1}{2}\lambda_2(1-c)x_2^2 \\ &\quad -\frac{1}{2}\lambda_2 d x_3^2+\frac{1}{2}\frac{\mu_2^2 d}{\lambda_2}. \end{aligned} \tag{23}$$

Apparently,

$$F(x(t)) \le \sup F(x(t)) = l_{\lambda_2,\mu_2} = \frac{1}{2}\frac{\mu_2^2 d}{\lambda_2}.$$

Thus,

$$D_t^q V_{\lambda_2,\mu_2}(x(t)) \le -\eta_2 V_{\lambda_2,\mu_2}+l_{\lambda_2,\mu_2}, \tag{24}$$

$$D_t^q\left(V_{\lambda_2,\mu_2}(t)-\frac{l_{\lambda_2,\mu_2}}{\eta_2}\right) \le -\eta_2\left(V_{\lambda_2,\mu_2}-\frac{l_{\lambda_2,\mu_2}}{\eta_2}\right). \tag{25}$$

According to Lemma 3, we have

$$V_{\lambda_2,\mu_2}(t)-\frac{l_{\lambda_2,\mu_2}}{\eta_2} \le \left(V_{\lambda_2,\mu_2}(0)-\frac{l_{\lambda_2,\mu_2}}{\eta_2}\right)E_q(-\eta_2 t^q),$$

$$t \ge 0. \tag{26}$$

Based on Definition 4, we can conclude that $\Psi^2_{\lambda_2,\mu_2}$ with $a>0, c<1, d>0, \lambda_2>0, \mu_2>\lambda_2 b$ is an MLAS and MLPIS for system (2) when $x_2<0$. This completes the proof.

Remark 1 If we take $q=0.98$, $a=10$, $b=28$, $c=0.4$, $d=8/3$, $\lambda_1=1$, $\mu_1=29$, $\lambda_2=1$, $\mu_2=32$, then

$$\Psi^1_{\lambda_1,\mu_1} = \left\{x(t)\in R^3 \left| 0.1x_1^2+x_2^2+(x_3-29)^2 \le (61.14)^2\right.\right\},$$
$$\Psi^2_{\lambda_2,\mu_2} = \left\{x(t)\in R^3 \left| 1.5x_1^2+x_2^2+(x_3-43)^2 \le (59.34)^2\right.\right\}.$$

Figure 14 shows phase portraits and MLAS of system (2).

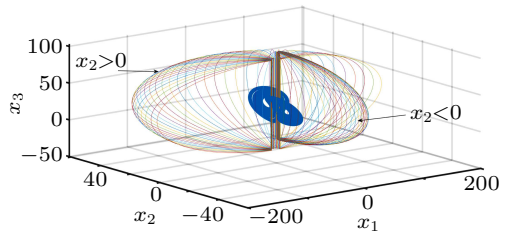


Fig. 14. The estimate MLAS of system (2) with $a=10$, $b=28$, $c=1.4$, $d=8/3$, $q=0.98$, $\lambda_1=1$, $\mu_1=43$; $\lambda_2=1$, $\mu_2=30$.

Remark 2 When $a=10$, $b=28$, $c=1.4$, $d=8/3$, $\lambda_1=\lambda_2=1$, $\mu_1=\mu_2=30$, it is obvious that $d\mu_1^2/\lambda_1\eta_1 > d\mu_2^2/\lambda_2\eta_2$, so the ellipsoid

$$\Psi^1_{\lambda_1,\mu_1} = \{x(t)\in R^3 \left| 0.2x_1^2+x_2^2+(x_3-30)^2 \le (63.24)^2\right.\}$$

is the MLAS and MLPIS for system (2) with different fractional order q. Figure 15 shows phase portraits and MLASs of system (2) with different fractional order q.

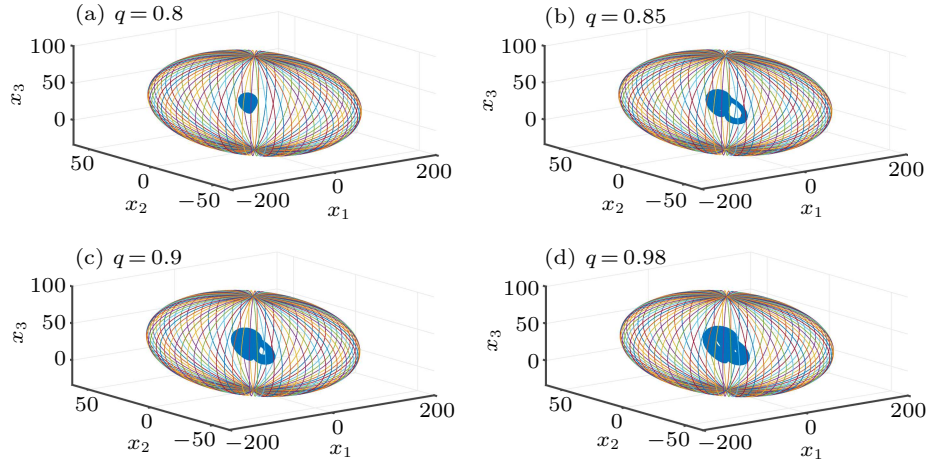


Fig. 15. The estimate MLAS of system (2) with $a=10$, $b=28$, $c=1.4$,$d=8/3$, (a) $q=0.8$, (b) $q=0.85$, (c) $q=0.9$, (d) $q=0.98$.

6. Forecasting of the FOFR system

The RC approach[34–36] comprises an input layer, a recurrent layer referred to as the reservoir (comprising many sparsely connected neurons) and an output layer. The connection weights of the input layer and the reservoir layer remain fixed after initialization, while the output weights are trainable and determined by solving a linear regression problem.

In the given context, $u(t) \in R^{M\times 1}$ represents the input value at time t of the time series, $w_{\text{in}} \in R^{N\times M}$ (with dimension M) signifies the connection weights between the input layer and the hidden layer, $w_{\text{res}} \in R^{N\times N}$ (with N representing the number of neurons) denotes the input-to-hidden layer connection weights, and $w_{\text{out}} \in R^{L\times N}$ (with dimension L) represents the output weights from the hidden layer to the output layer. The state transition equation is expressed as follows, represented by equation

$$\begin{cases} r(t) = \gamma \tanh(w_{\text{in}} u(t) + w_{\text{res}} r(t-1)) + (1-\gamma) r(t-1), \\ y(t) = w_{\text{out}} r(t). \end{cases} \tag{27}$$

In this equation, $r(t)$ and $y(t)$ represent the state of the reservoir and output, respectively. γ denotes the leaky rate, incorporating the previous state into the current one. The $\tanh(\cdot)$ signifies the activation function within the reservoir.

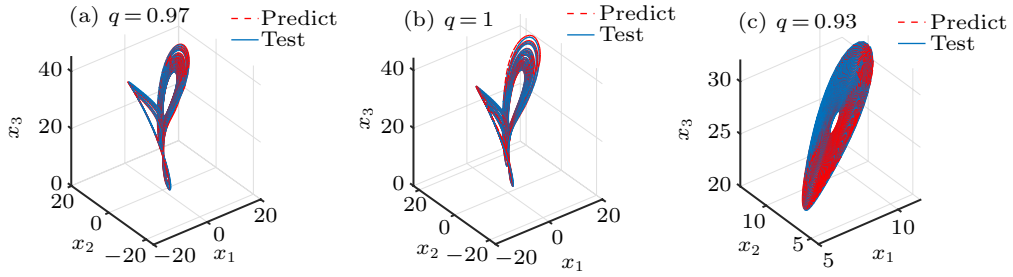


Fig. 16. Phase diagrams of predicted data and test data: (a) $q = 0.97$, (b) $q = 1$, and (c) $q = 0.93$.

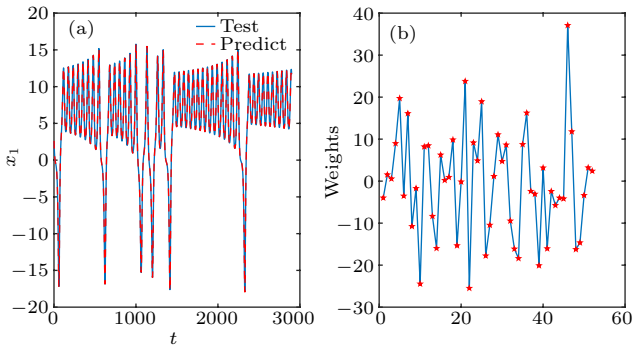


Fig. 17. Training and prediction results of the RC model for $x_1(t)$ state variable of the model (2) at $q = 0.97$. (a) The test data in blue color versus predicted data in red color. (b) The weights after the completion of training.

We study the time series solution of the proposed model in Eq. (2) by employing the RC forecasting approach. The generated time series consists of 10^4 data points representing a state variable. The first 7000 items is dedicated to training dataset while another 3000 is reserved for testing. To improve the reliability of the prediction, we remove the first 100 elements from both training data and testing data. Moreover, the number of RC nodes is limited to 52, while accounting only three cases of fractional order q. Figure 16 shows the phase diagrams of predicted data and test data. Figures 17–19 exhibit both results, the training and prediction processes at $q = 0.97$ given numerous values of state variables for the system (2). Figures 20–22 show the results of the training and prediction at $q = 1$, for the state variables of the system (2). Additionally, figures 23–25 illustrate the results from training and prediction processes at $q = 0.93$ for the state variables of the system (2). We use LSTM technique for the purpose of forecasting process of the financial time series. In so doing, the dataset is separated into the training dataset chosen from the first 7000, while a validation dataset for the other 3000. Examples of the obtained results are illustrated in Figs. 26–28. It is evident that the prediction process based on RC produces superior accuracy over extended durations and demonstrates notably reduced forecasting errors when contrasted with the LSTM method.

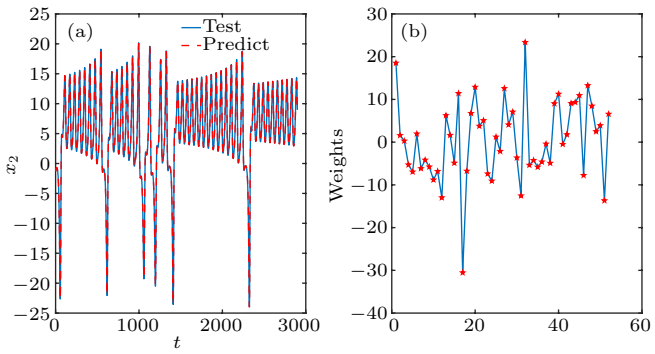


Fig. 18. Training and prediction results of the RC model for $x_2(t)$ state variable of the model (2) at $q = 0.97$. (a) The test data in blue color versus predicted data in red color. (b) The weights after the completion of training.

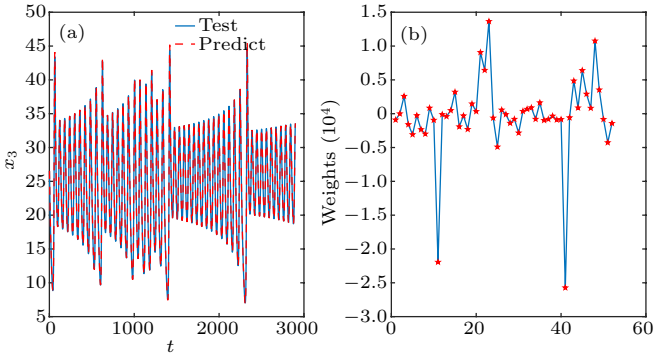


Fig. 19. Training and prediction results of the RC model for $x_3(t)$ state variable of the model (2) at $q = 0.97$. (a) The test data in blue color versus predicted data in red color. (b) The weights after the completion of training.

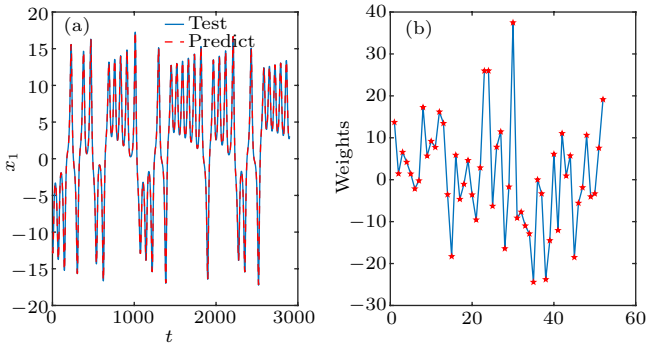


Fig. 20. Training and prediction results of the RC model for $x_1(t)$ state variable of the model (2) at $q = 1$. (a) The test data in blue color versus predicted data in red color. (b) The weights after the completion of training.

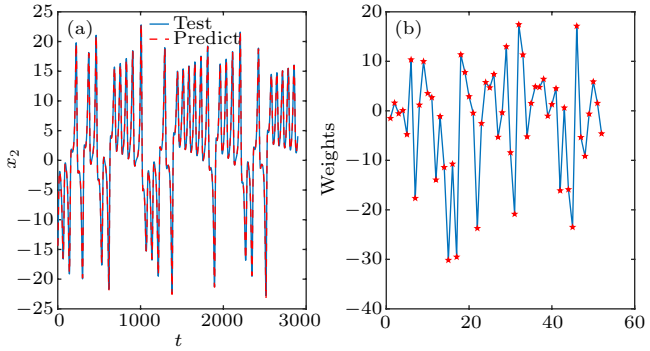


Fig. 21. Training and prediction results of the RC model for $x_2(t)$ state variable of the model (2) at $q = 1$. (a) The test data in blue color versus predicted data in red color. (b) The weights after the completion of training.

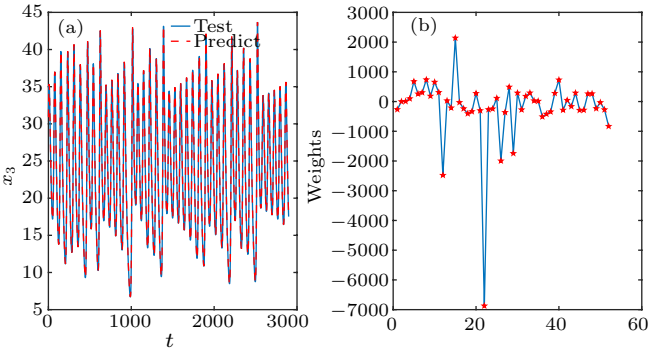


Fig. 22. Training and prediction results of the RC model for $x_3(t)$ state variable of the model (2) at $q = 1$. (a) The test data in blue color versus predicted data in red color. (b) The weights after the completion of training.

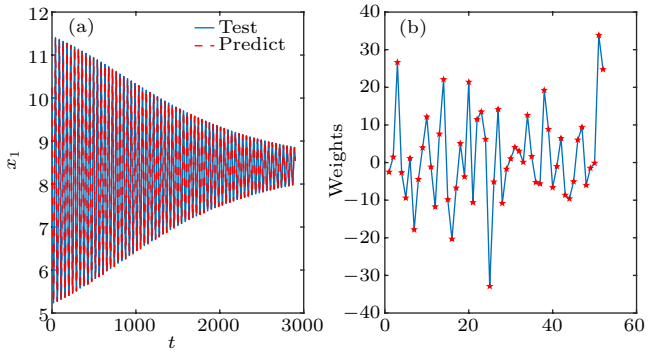


Fig. 23. Training and prediction results of the RC model for $x_1(t)$ state variable of the model (2) at $q = 0.93$. (a) The test data in blue color versus predicted data in red color. (b) The weights after the completion of training.

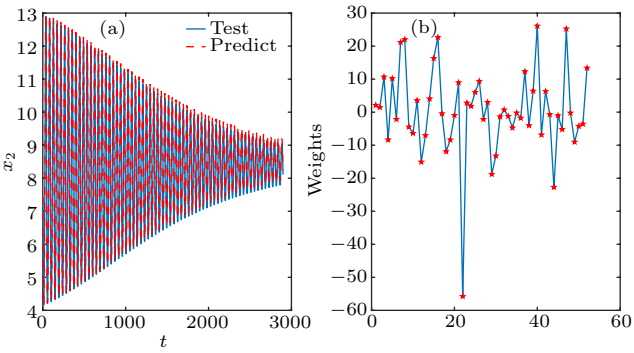


Fig. 24. Training and prediction results of the RC model for $x_2(t)$ state variable of the model (2) at $q = 0.93$. (a) The test data in blue color versus predicted data in red color. (b) The weights after the completion of training.

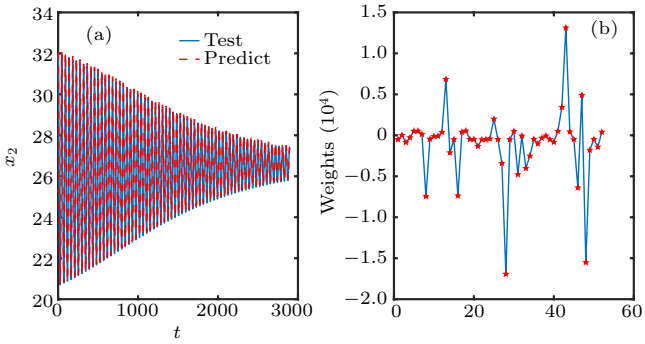


Fig. 25. Training and prediction results of the RC model for $x_3(t)$ state variable of the model (2) at $q = 0.93$. (a) The test data in blue color vs predicted data in red color. (b) The weights after the completion of training.

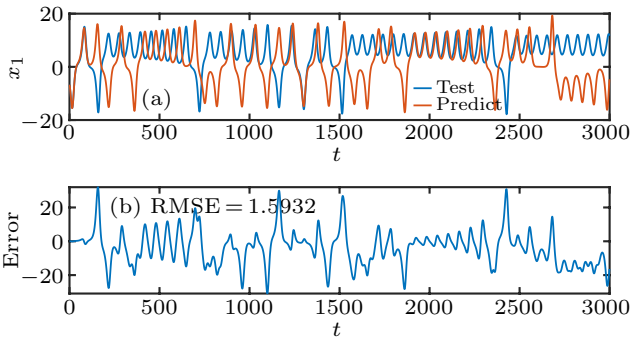


Fig. 26. Training and prediction results of the LSTM model for $x_1(t)$ state variable of the model (2) at $q = 0.97$. (a) The test data in blue color versus predicted data in red color. (b) The error between test and predicted time series.

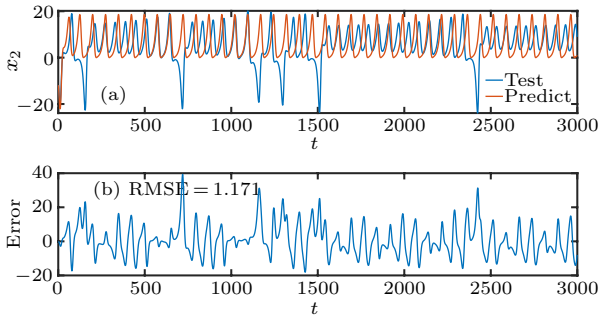


Fig. 27. Training and prediction results of the LSTM model for $x_2(t)$ state variable of the model (2) at $q = 0.97$. (a) The test data in blue color versus predicted data in red color. (b) The error between test and predicted time series.

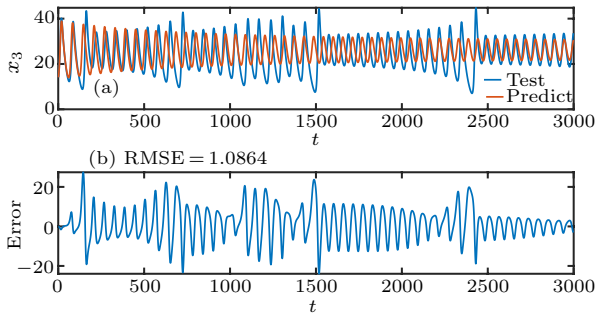


Fig. 28. Training and prediction results of the LSTM model for $x_3(t)$ state variable of the model (2) at $q = 0.97$. (a) The test data in blue color versus predicted data in red color. (b) The error between test and predicted time series.

Tables 1 and 2 look closer into the performance of the two approaches, specifically in terms of RMSE and MAE across various cases of q and different state variables.

Table 1. RC forecasting scheme versus LSTM approach (RMSE).

Predicted series	RMSE (RC)	RMSE (LSTM)
$x_1(t), q = 0.97$	0.011422	1.5932
$x_2(t), q = 0.97$	0.014704	1.1710
$x_3(t), q = 0.97$	0.015034	1.0864
$x_1(t), q = 1$	0.013542	1.2135
$x_2(t), q = 1$	0.011314	1.2741
$x_3(t), q = 1$	0.023641	1.3557
$x_1(t), q = 0.93$	0.06416	1.8724
$x_2(t), q = 0.93$	0.084321	2.0645
$x_3(t), q = 0.93$	0.06127	1.9987

Table 2. RC forecasting scheme versus LSTM approach (MAE).

Predicted series	MAE (RC)	MAE (LSTM)
$x_1(t), q = 0.97$	0.009182	1.1547
$x_2(t), q = 0.97$	0.011755	1.1342
$x_3(t), q = 0.97$	0.012711	1.0642
$x_1(t), q = 1$	0.010247	1..0677
$x_2(t), q = 1$	0.010112	1.1631
$x_3(t), q = 1$	0.014765	1.2163
$x_1(t), q = 0.93$	0.043276	1.6772
$x_2(t), q = 0.93$	0.062181	1.9921
$x_3(t), q = 0.93$	0.042182	1.9741

7. Conclusion

In this paper, we proposed an FOFR system with one absolute function term. Based on the ADM algorithm, we investigated the complexity and chaotic behavior of the system using various techniques such as phase portraits, bifurcation diagrams, Lyapunov exponent spectrum, SE, C_0, and 0–1 test. Moreover, we investigated the stability of equilibrium points and explored techniques for controlling chaos. Furthermore, we provided estimations of the global MLAS and MLPIS for the FOFR model. Additionally, we presented a proficient machine learning method capable of forecasting the temporal evolution of the observed nonlinear behaviors within the proposed system, and compared with the RC-based model and the LSTM technique. The analytical results are substantiated by numerical simulations.

Since the two important factors of time delay and fractional incommensurate-order in financial systems, the study of financial systems with time delay and fractional incommensurate-order is of great significance for understanding and managing financial markets. As such, our future work will focus on this issue.

Appendix A

Using ADM, the FOFR system (2) is decomposable into the following form:

$$\begin{bmatrix} x_1(t) \\ x_2(t) \\ x_3(t) \end{bmatrix} = \begin{bmatrix} x_1(t_0) \\ x_2(t_0) \\ x_3(t_0) \end{bmatrix} + J^q_{t_0} \begin{bmatrix} a(x_1 - x_2) \\ bx_1 - x_2 - c\,|x_2| \\ -dx_3 \end{bmatrix} + J^q_{t_0} \begin{bmatrix} 0 \\ -x_1x_3 \\ x_1x_2 \end{bmatrix}. \tag{A1}$$

The results of the decomposition of the nonlinear terms are shown below, where the subscripts indicate the nonlinear terms being decomposed:

$$\begin{aligned}
A^0_{-x_1x_3} &= -x_1^0x_3^0, \\
A^1_{-x_1x_3} &= -x_1^1x_3^0 - x_1^0x_3^1, \\
A^2_{-x_1x_3} &= -x_1^2x_3^0 - x_1^1x_3^1 - x_1^0x_3^2, \\
A^3_{-x_1x_3} &= -x_1^3x_3^0 - x_1^2x_3^1 - x_1^1x_3^2 - x_1^0x_3^3, \\
A^4_{-x_1x_3} &= -x_1^4x_3^0 - x_1^3x_3^1 - x_1^2x_3^2 - x_1^1x_3^3 - x_1^0x_3^4, \\
A^5_{-x_1x_3} &= -x_1^5x_3^0 - x_1^4x_3^1 - x_1^3x_3^2 - x_1^2x_3^3 - x_1^1x_3^4 - x_1^0x_3^5,
\end{aligned} \tag{A2}$$

$$\begin{aligned}
A^0_{x_1x_2} &= x_1^0x_2^0, \\
A^1_{x_1x_2} &= x_1^1x_2^0 + x_1^0x_2^1, \\
A^2_{x_1x_2} &= x_1^2x_2^0 + x_1^1x_2^1 + x_1^0x_2^2, \\
A^3_{x_1x_2} &= x_1^3x_2^0 + x_1^2x_2^1 + x_1^1x_2^2 + x_1^0x_2^3, \\
A^4_{x_1x_2} &= x_1^4x_2^0 + x_1^3x_2^1 + x_1^2x_2^2 + x_1^1x_2^3 + x_1^0x_2^4, \\
A^5_{x_1x_2} &= x_1^5x_2^0 + x_1^4x_2^1 + x_1^3x_2^2 + x_1^2x_2^3 + x_1^1x_2^4 + x_1^0x_2^5,
\end{aligned} \tag{A3}$$

The first set of coefficients b^0_j $(j = 1,2,3)$:

$$\begin{aligned}
b^0_1 &= x_1(t_0), \\
b^0_2 &= x_2(t_0), \\
b^0_3 &= x_3(t_0).
\end{aligned} \tag{A4}$$

The other sets of coefficient respectively are

$$\begin{aligned}
b^1_1 &= a(b^0_2 - b^0_1), \\
b^1_2 &= bb^0_1 - b^0_2 - c\,|b^0_2| - b^0_1b^0_3, \\
b^1_3 &= -db^0_3 + b^0_1b^0_2, \\
b^2_1 &= a(b^1_2 - b^1_1),
\end{aligned} \tag{A5}$$

$$
\begin{aligned}
b_2^2 &= bb_1^1 - b_2^1 - c\left|b_2^1\right| - b_1^1 b_3^0 - b_1^0 b_3^1,\\
b_3^2 &= -db_3^1 + b_1^2 b_2^0 + b_1^0 b_2^1,
\end{aligned}
\tag{A6}
$$

$$
\begin{aligned}
b_1^3 &= a(b_2^2 - b_1^2),\\
b_2^3 &= bb_1^2 - b_2^2 - c\left|b_2^2\right| - b_1^2 b_3^0 - b_1^1 b_3^1 \frac{\Gamma(2q+1)}{\Gamma^2(q+1)} - b_1^0 b_3^2,\\
b_3^3 &= -db_3^2 + b_1^2 b_2^0 + b_1^1 b_2^1 \frac{\Gamma(2q+1)}{\Gamma^2(q+1)} + b_1^0 b_2^2,
\end{aligned}
\tag{A7}
$$

$$
\begin{aligned}
b_1^4 &= a(b_2^3 - b_1^3),\\
b_2^4 &= bb_1^3 - b_2^3 - c\left|b_2^3\right| - b_1^3 b_3^0\\
&\quad - (b_1^2 b_3^1 + b_1^1 b_3^2)\frac{\Gamma(3q+1)}{\Gamma(q+1)\Gamma(2q+1)} - b_1^0 b_3^3,\\
b_3^4 &= -db_3^3 + b_1^3 b_2^0 + (b_1^2 b_2^1 + b_1^1 b_2^2)\\
&\quad \times \frac{\Gamma(3q+1)}{\Gamma(q+1)\Gamma(2q+1)} + b_1^0 b_2^3,
\end{aligned}
\tag{A8}
$$

$$
\begin{aligned}
b_1^5 &= a(b_2^4 - b_1^4),\\
b_2^5 &= bb_1^4 - b_2^4 - c\left|b_2^4\right| - b_1^4 b_3^0\\
&\quad - (b_1^3 b_3^1 + b_1^1 b_3^3)\frac{\Gamma(4q+1)}{\Gamma(q+1)\Gamma(3q+1)}\\
&\quad - b_1^2 b_3^2 \frac{\Gamma(4q+1)}{\Gamma^2(2q+1)} - b_1^0 b_3^4,\\
b_3^5 &= -db_3^4 + b_1^4 b_2^0 + (b_1^3 b_2^1 + b_1^1 b_2^3)\frac{\Gamma(4q+1)}{\Gamma(q+1)\Gamma(3q+1)}\\
&\quad + b_1^2 b_2^2 \frac{\Gamma(4q+1)}{\Gamma^2(2q+1)} + b_1^0 b_2^4,
\end{aligned}
\tag{A9}
$$

$$
\begin{aligned}
b_1^6 &= a(b_2^5 - b_1^5),\\
b_2^6 &= bb_1^5 - b_2^5 - c\left|b_2^5\right| - b_1^5 b_3^0\\
&\quad - (b_1^4 b_3^1 + b_1^1 b_3^4)\frac{\Gamma(5q+1)}{\Gamma(q+1)\Gamma(4q+1)}\\
&\quad - (b_1^3 b_3^2 + b_1^2 b_3^3)\frac{\Gamma(5q+1)}{\Gamma(2q+1)\Gamma(3q+1)} - b_1^0 b_3^5,\\
b_3^6 &= -db_3^5 + b_1^5 b_2^0 + (b_1^4 b_2^1 + b_1^1 b_2^4)\frac{\Gamma(5q+1)}{\Gamma(q+1)\Gamma(4q+1)}\\
&\quad + (b_1^3 b_2^2 + b_1^2 b_2^3)\frac{\Gamma(5q+1)}{\Gamma(2q+1)\Gamma(3q+1)} + b_1^0 b_2^5.
\end{aligned}
\tag{A10}
$$

Combining the above derivations, the solution of the system can be obtained as

$$
\begin{aligned}
x_1(t) &= b_1^0 + b_1^1\frac{h^q}{\Gamma(q+1)} + b_1^2\frac{h^{2q}}{\Gamma(2q+1)} + b_1^3\frac{h^{3q}}{\Gamma(3q+1)}\\
&\quad + b_1^4\frac{h^{4q}}{\Gamma(4q+1)} + b_1^5\frac{h^{5q}}{\Gamma(5q+1)} + b_1^6\frac{h^{6q}}{\Gamma(6q+1)},\\
x_2(t) &= b_2^0 + b_2^1\frac{h^q}{\Gamma(q+1)} + b_2^2\frac{h^{2q}}{\Gamma(2q+1)} + b_2^3\frac{h^{3q}}{\Gamma(3q+1)}\\
&\quad + b_2^4\frac{h^{4q}}{\Gamma(4q+1)} + b_2^5\frac{h^{5q}}{\Gamma(5q+1)} + b_2^6\frac{h^{6q}}{\Gamma(6q+1)},\\
x_3(t) &= b_3^0 + b_3^1\frac{h^q}{\Gamma(q+1)} + b_3^2\frac{h^{2q}}{\Gamma(2q+1)} + b_3^3\frac{h^{3q}}{\Gamma(3q+1)}\\
&\quad + b_3^4\frac{h^{4q}}{\Gamma(4q+1)} + b_3^5\frac{h^{5q}}{\Gamma(5q+1)} + b_3^6\frac{h^{6q}}{\Gamma(6q+1)},
\end{aligned}
$$

where h denotes the step size.

Acknowledgements

Project jointly supported by the National Natural Science Foundation of China (Grant No. 12372013), Program for Science and Technology Innovation Talents in Universities of Henan Province, China (Grant No. 24HASTIT034), the Natural Science Foundation of Henan Province, China (Grant No. 232300420122), the Humanities and Society Science Foundation from the Ministry of Education of China (Grant No. 19YJCZH265), China Postdoctoral Science Foundation (Grant No. 2019M651633), First Class Discipline of Zhejiang-A (Zhejiang University of Finance and Economics-Statistics), the Collaborative Innovation Center for Data Science and Big Data Analysis (Zhejiang University of Finance and Economics-Statistics).

References

[1] Podlubny I *1999 Fractional differential equations* (New York: Academic Press) pp. 41–120
[2] Petráš I 2011 *Fractional-Order Nonlinear Systems: Modeling, Analysis and Simulation* (Berlin: Springer Science & Business Media) pp. 7–42
[3] Yuan L, Zheng S and Wei Z 2022 *Eur. Phys. J. Spec. Top.* **231** 2477
[4] Chen L, Wu X, António M L, Li X, Li P and Wu R 2023 *Commun. Nonlinear Sci. Numer. Simul.* **125** 107365
[5] Zhou X, Jiang D, Nkapkop J, Ahmad M, Fossi J, Tsafack N and Wu J 2024 *Chin. Phys. B* **33** 040506
[6] Jin M X, Sun K H and He S B 2023 *Chin. Phys. B* **32** 060501
[7] Zhang Y, Xiao M, Cao J and Zheng W 2022 *IEEE Trans. Syst. Man Cyber.: Syst.* **52** 1731
[8] Xu C, Liu Z, Liao M and Yao L 2022 *Expert Syst. Appl.* **199** 116859
[9] El-Mesady A, Elsonbaty A and Adel W 2022 *Chaos, Solitons and Fractals* **164** 112716
[10] Partohaghighi M, Yusuf A and Bayram M 2022 *Int. J. Appl. Comput. Math.* **8** 86
[11] Chen L, Yin H, Huang T, Yuan L, Zheng S and Yin L 2020 *Neural Netw.* **125** 174
[12] Cui L, Luo W and Ou Q 2021 *Chin. Phys. B* **30** 020501
[13] He S, Wang H and Sun K 2022 *Chin. Phys. B* **31** 060501
[14] Vignesh D, He S and Banerjee S 2023 *Appl. Math. Comput.* **455** 128111
[15] Tang Z, He S, Wang H, Sun K, Yao Z and Wu X 2024 *Chin. Phys. B* **33** 030503
[16] Wang X, Xu B, Shi P and Li S 2022 *IEEE Tran. Neural Net. Lear. Syst.* **33** 445
[17] Wu X, Fu L, He S, Yao Z, Wang H and Han J 2023 *Resul. Phys.* **52** 106866
[18] Leonov G, Bunin A and Koksch N 1987 *Z. Angew. Math. Mech.* **67** 649
[19] Leonov G and Kuznetsov N 2013 *Int. J. Bifurc. Chaos* **23** 1330002
[20] Swinnerton-Dyer P 2001 *Phys. Lett. A* **281** 161
[21] Liao X 2004 *Sci. China Ser. E, Inform. Sci.* **34** 1404
[22] Jian J, Wu K and Wang B 2020 *Physica A* **540** 123166
[23] Peng Q and Jian J 2021 *Chaos, Solitons and Fractals* **150** 111072
[24] Ren L, Lin M, Abdulwahab A, Ma J and Saberi-Nik H 2023 *Chaos, Solitons and Fractals* **169** 113275
[25] Zhang X, Liu X, Zheng Y and Liu C 2013 *Chin. Phys. B* **22** 030509
[26] Tacha O, Volos C, Kyprianidis I, Stouboulos I, Vaidyanathan S and Pham V 2016 *Appl. Math. Comput.* **276** 200
[27] Tacha O, Munoz-Pacheco J, Zambrano-Serrano E, Stouboulos I and Pham V 2018 *Nonlinear Dyn.* **94** 1303
[28] Jahanshahi H, Sajjadi S, Bekiros S and Aly A 2021 *Chaos, Solitons and Fractals* **144** 110698
[29] Festag S, Denzler J and Spreckelsen C 2022 *J. Biomed. Inform.* **129** 104058

[30] Maleki M, Mahmoudi M, Wraith D and Pho K 2022 *Travel Med. Infect. Dis.* **37** 101742
[31] Puri C, Kooijman G, Vanrumste B and Luca S 2022 *IEEE J Biomed. Health Inform.* **26** 6126
[32] Chimmula V and Zhang L 2022 *Chaos, Solitons and Fractals* **135** 109864
[33] Wang W, Shao J and Jumahong H 2023 *Sci. Rep.* **13** 20359
[34] Maass W, Natschläger T and Markram H 2002 *Neural Comput.* **14** 2531
[35] Jaeger H and Haas H 2004 *Science* **304** 78
[36] Du C, Cai F, Zidan M, Ma W, Lee S and Lu W 2017 *Nat. Commun.* **8** 1
[37] Song Q, Zhao X, Feng Z, An Y and Song B 2021 *CCDC* 3893–3897
[38] Na X, Ren W, Liu M, Han M 2023 *IEEE Trans. Neural Netw. Lear. Syst.* **34** 9302
[39] Staniczenko P, Lee C and Jones N 2009 *Phys. Rev. E* **79** 011915
[40] Shen E, Cai Z and Gu F 2005 *Appl. Math. Mech.* **26** 1188
[41] Gottwald G and Melbourne I 2004 *Proc. Roy. Soc. A-Math. Phys. Eng. Sci.* **460** 603
[42] Muhamad D, Aceng S, Zheng S, Khaled B, Sundarapandian V, Mohamed M and Mamat M 2023 *Chaos, Solitons and Fractals* **177** 114283
[43] Cherruault Y and Adomian G 1993 *Math. Comput. Model.* **18** 103